Translational Oncology 56 (2025) 102382

Contents lists available at ScienceDirect

Translational Oncology

journal homepage: www.elsevier.com/locate/tranon

Original Research

Raddeanin A exerts potent efficacy against non-small cell lung cancer by inhibiting cyclin-dependent kinase 6

Xian Wang [a,b,c,#], Xiao Lin [a,#], Yuxin Liu [a], Chunbo Ma [a], Mengchu Liu [a], Jiayu Bai [a], Yihan Ye [a], Chengguang Zhao [b], Lehe Yang [a,*], Xiaoying Huang [a,*], Liangxing Wang [a,*]

[a] Pulmonary Division, the First Affiliated Hospital of Wenzhou Medical University, Wenzhou Key Laboratory of Interdiscipline and Translational Medicine, Wenzhou Key Laboratory of Heart and Lung, Wenzhou, Zhejiang 325035, China
[b] School of Pharmaceutical Sciences, Wenzhou Medical University, Wenzhou, Zhejiang 325035, China
[c] Shanghai Fengxian District Central Hospital, No. 6600, Nanfeng Highway, Fengxian District, Shanghai 201499, China

ARTICLE INFO

Keywords:
Raddeanin A
NSCLC
CDK6
Cycle arrest
inhibitor

ABSTRACT

Purpose: The aim of this study was to investigate the anti-tumor effects and mechanisms of Raddeanin A in NSCLC in vitro and in vivo.
Methods: The effects of Raddeanin A on cell cycle progression, proliferation, migration and invasion of NSCLC were assessed by flow cytometry and cell biological assays in multiple NSCLC cell lines. To identify possible targets of Raddeanin A in NSCLC, we employed a multifaceted approach incorporating network pharmacology, molecular docking, and molecular dynamics simulation, along with additional techniques such as SPR (Surface Plasmon Resonance), Co-IP (Co-Immunoprecipitation), and immunofluorescence. In vivo effects were investigated using a nude mouse xenograft tumor model.
Results: Raddeanin A inhibits NSCLC cell survival, inhibits invasion and migration and causes cell cycle arrest in G1 phase. Raddeanin A impacts NSCLC cellular activity by inhibiting CDK6, leading to anti-tumor effects. Molecular analysis confirms that the tight binding between Raddeanin A and CDK6, facilitated by specific hydrogen bonds at binding sites including VAL-101, HIS-100, GLN-149, LYS-147, THR-182, VAL-180, and ALA-23, stabilizes within the 40–100 ns interval. In a nude mouse xenograft tumor model, Raddeanin A also demonstrated an inhibitory effect on NSCLC tumor growth.
Conclusions: Raddeanin A blocks the cell cycle in G1 phase by inhibiting CDK6. Raddeanin A is expected to be a novel antitumor agent against NSCLC.

Introduction

The most common type of lung cancer is Non-small cell lung cancer (NSCLC), which has a high degree of morphological heterogeneity [1]. Despite recent insights into the pathogenesis of lung cancer, NSCLC remains highly aggressive and lethal [2], with an overall survival of <5 years. Molecularly targeted therapies and immunotherapies for NSCLC developed over the past two decades have shown significant efficacy; however, current therapies do not arrest progression in the majority of NSCLC cases [3]. From this perspective, it is particularly important to identify breakthrough therapies for NSCLC.

One potential target of anti-cancer agents are cyclin-dependent kinases (CDKs), which are important bridges between extracellular and intracellular signaling pathways that play key roles in regulating gene transcription and cell division [4–6]. Uncontrolled cell proliferation is the core pathological process of cancer, and the dysregulation of cell

Abbreviations: **RA**, Raddeanin A; **NSCLC**, non-small cell lung cancers; **Rb**, Retinoblastoma; **CDKs**, cyclin-dependent kinases; **MTT**, Methyl thiazolyl tetrazolium; **DAPI**, 4,6-diamidino-2-phenylindole dihydro-chloride; **DMEM**, Dulbecco minimum essential medium; **EdU**, 5-ethynyl-2 '- deoxyuridine; **FBS**, fetal bovine serum; **GAPDH**, glyceraldehyde 3-phosphate dehydrogenase; **HE**, hematoxylin-eosin staining; **IC_{50}**, the half maximal inhibitory concentrations; **MMP2**, matrix metallopeptidase 2; **OD**, optical density; **PBS**, phosphate-buffered saline; **PVDF**, polyvinylidene fluoride; SD, standard deviation; **SDS-PAGE**, sodium dodecyl sulfate-polyacrylamidegel; **SPR**, Surface Plasmon Resonance; **CO-IP**, Co-immunoprecipitation; **BSA**, bovine serum albumin; **PFA**, paraformaldehyde.

* Corresponding authors.
E-mail addresses: yanglehe@wmu.edu.cn (L. Yang), huangxiaoying@wmu.edu.cn (X. Huang), wangliangxing@wzhospital.cn (L. Wang).
# Authors equally contributed to this work.

https://doi.org/10.1016/j.tranon.2025.102382
Received 31 October 2024; Received in revised form 25 March 2025; Accepted 28 March 2025

cycle mechanisms and activation of CDKs is one mechanism to mediate cell cycle progression [7]. Phosphorylation and inactivation of the tumor suppressor retinoblastoma (Rb) can be regulated by CDK4/6 and can affect cell cycle progression [8]. Therefore, CDK4/6 has served as a target of small-molecule inhibitors for the treatment of cancer.

The CDK4/6 gene is widely expressed in various tumors, and in most tumor types, its expression differs markedly from that of normal tissues. The primary battleground for CDK4/6 inhibitors is currently HR+/HER2- breast cancer, but efforts are underway to explore their role in other malignancies [9]. Many studies have shown that CDK4/6 inhibitors can increase the sensitivity of acute myeloid leukemia cells to drugs [10]. Numerous basic experiments and early clinical trials have demonstrated the significant anti-lung cancer efficacy of CDK4/6 inhibitors [11–13], with their safety and anti-tumor activity preliminarily validated. The potential mechanisms include inducing cell cycle arrest in the G1 phase and promoting DNA damage [14,15]. Currently, the CDK4/6 inhibitor trilaciclib (Cosela) is available for clinical use [16,17], but it is only approved for the treatment of extensive-stage small cell lung cancer and not for NSCLC. Therefore, identifying and exploring CDK4/6 inhibitors with therapeutic potential for NSCLC is of significance importance.

The herb *Anemone raddeana regel* is a precious folk medicine in China. It has the effects of removing wind and dampness, dispelling cold and pain and reducing carbuncles and swelling [18]. The natural product Raddeanin A is a traditional Chinese medicine monomer that can be extracted from *Anemone raddeana regel.* Multiple studies have shown that Raddeanin A can inhibit the development of various forms of cancer, such as breast cancer [19], liver cancer [20], stomach cancer [21] and colorectal cancer [22] and that it has significant anti-tumor activity [23]. Several reports have investigated the effects of this compound in lung cancer cells [24,25], but more research is needed, especially in terms of its anti-tumor activity in vivo. The aim of this study, therefore, was to uncover the role of Raddeanin A in NSCLC, both in vivo and in vitro.

Materials and methods

Cell lines and culture

Human NSCLC cell lines were obtained from the Chinese Academy of Sciences (Shanghai, China). PC-9, A549 and HCC827 cells were cultured in DMEM medium (Thermo Fisher Scientific, Waltham, MA, USA) supplemented with 10 % FBS. H1299 and H1975 cells were cultured in RPMI 1640 medium (Thermo Fisher Scientific) supplemented with 10 % FBS. All NSCLC cells required for this study were cultured in a humidified incubator at 37°C in a 5 % CO_2 atmosphere.

Antibodies and reagents

Raddeanin A (Jingwei Biotechnology, Nantong, China) was dissolved in dimethyl sulfoxide (DMSO). Primary antibodies against CDK4, CDK6, cyclin D1, Rb, P-Rb, Snail, MMP2, E-calmodulin, vimentin and GAPDH were obtained from Cell Signaling Technology (Danvers, MA, USA). Horseradish peroxidase-conjugated donkey anti-rabbit IgG and goat anti-mouse IgG secondary antibodies were obtained from Santa Cruz Biotechnology (Santa Cruz, CA, USA). Additional materials included an enhanced chemiluminescence kit from Bio Rad Laboratory (Hercules, California, USA), a protein extraction kit (Boster Biotechnology, Wuhan, China), Bradford protein assay reagent, PVDF membrane, acrylamide (30 %), Coomassie brilliant blue, pre-stained protein markers, and skimmed milk powder. This study used.

Methyl thiazolyl tetrazolium (MTT) assay

Determination of the proliferative capacity of NSCLC cells was performed using an MTT assay kit (Sigma Aldrich, St. Louis, MO, USA). Cells were inoculated into 96-well plates at a standard of 4.5×10^3 cells/well and incubated for 1 day before treatment with drugs. Drug concentrations ranging from 0 μM to 10 μM (specifically 0, 0.01, 0.05, 0.1, 0.25, 0.5, 1, 2.5, 5, and 10 μM) were added to each well, followed by an incubation period of 48 h. Subsequently, MTT solution was added and the plate continued to be incubated for 4 h. The absorbances were read with a plate reader, and GraphPad Pro Prism 8.0 (San Diego, CA, USA) was employed to process the data and calculate the IC_{50} values of the drugs.

Colony formation assay

NSCLC cells were inoculated in 6-well plates at a density of 1000 cells per well. After the cells were attached to the plate, DMSO or Raddeanin A (1, 2 or 4 μM) were added, and the plates were placed into the incubator. The medium was changed once every three days, and the proliferation of NSCLC cells was observed. The culture was terminated when the cell colonies in the control wells grew throughout the wells. Each well was washed three times with PBS, and the cells were fixed with PFA for 30 min. Finally, crystal violet solution was added, and the cells were stained for 20 min and then photographed under light microscopy.

5-Ethynyl-2′-deoxyuridine (EdU) staining

NSCLC cells are evenly laid on a 24-well plate, and the next step can be carried out after they adhere to the wall. Cells were treated with Raddeanin A at indicated concentrations (0, 1, 2, 4 μM) for 24 h, appropriately diluted EdU labeling reagent (Beyotime Biotechnology, Beijing, China) was added to each well and allowed to react for 2 h. After removing the medium, 4 % PFA was used to fix the cells for 30 min. 0.1 % Triton X-100 was added to the cells (incubated on ice for 30 min) to permeabilise the cells. Cells were stained with BeyoClick™ EdU-555 for 30 min under light-avoidance conditions. Finally, cell nuclei were counterstained with Hoechst 33,342 (B2261, Sigma, USA) for 10 min, and images were obtained with confocal microscopy.

Transwell assay

The NSCLC cell migration and invasion assay requires the transwell chamber manufactured by BD Biosciences (USA). Matrix gel (BD Biosciences) was diluted 1:8 and then spread in the upper chamber. Cell suspension samples (200 μL containing 20,000 cells) were added to the upper chamber while culture medium containing 10 % FBS (600 μL) was added to the lower chamber. After 24 h, the medium in the upper chamber was changed to serum-free medium and cells were treated with Raddeanin A at indicated concentrations (0, 1, 2, 4 μM) in the upper chamber. After an incubation period of 24 h, the cells on the chamber membranes were fixed with 4 % PFA, stained with crystal violet and photographed under light microscopy. For migration assays, the same procedure was followed except that matrix gel was not added to the upper chamber.

Wound healing assay

NSCLC cells were evenly distributed on 6-well plates, after they adhere to the wall, cells were treated with Raddeanin A at indicated concentrations (0, 1, 2, 4 μM) for 24 h. Gaps were generated with sterile 10 μL pipette tips, and the cells were photographed at 0 h, 24 h and 48 h after drug treatment.

Western blot analysis

The primary antibodies utilized for Western Blot analysis included anti-E-Cadherin (#3195, Cell Signaling Technology, 1:1000), anti-Snail (#3879, Cell Signaling Technology, 1:1000), anti-Vimentin (#5741,

Cell Signaling Technology, 1:1000), anti-MMP2 (#4022, Cell Signaling Technology, 1:1000), anti-CDK4 (ab199728, Abcam, 1:1000), anti-Rb (ab226979, Abcam, 1:1000), anti-CDK6 (ab151247, Abcam, 1:1000), anti-CyclinD1 (ab226977, Abcam, 1:1000), anti-Rb (phospho S807) (ab184796, Abcam, 1:1000), and anti-GAPDH (#5174, Cell Signaling Technology, 1:2000). For immunofluorescence (IF), anti-CDK6 (ab151247, Abcam, 1:200) was employed. In the co-immunoprecipitation (Co-IP) assay, anti-CDK6 (ab151247, Abcam) and anti-CyclinD1(ab226977, Abcam) were used. Goat anti-rabbit IgG-HRP (Biosharp, 1:10,000) was used as the secondary antibody, and the ECL ultra sensitive test kit (Yeasen Biotechnology) was applied for detection.The NSCLC cells were uniformly spread in the 6-well plate. After treating with Raddeanin A at indicated concentrations (0, 1, 2, 4 μM) for 24 h, the cells were washed, and proteins were extracted by adding a lysis buffer to the plate. The extracted proteins were separated with 10 % or 12 % SDS-PAGE and then transferred electrophoretically to PVDF membranes. 5 % skimmed milk was used to seal the membranes for 2 h, followed by overnight incubation at 4°C with the specific primary antibody. The secondary antibody was then incubated with the membrane for 1 h at room temperature and then developed with ECL reagent. The resulting band intensities were analyzed using ImageJ software.

Flow cytometry

Flow cytometric analyses were performed using a cell cycle analysis kit (BD Pharmingen, Franklin Lakes, NJ, USA). Cells were treated with Raddeanin A at indicated concentrations (0, 1, 2, 4 μM) for 24 h. After digesting drug-treated cells, the reagent was added and incubate the cells for 20 min under conditions protected from light. Data were analyzed using FlowJo software (Ashland, OR, USA). Flow cytometry is an experimental tool used to detect cycle changes in NSCLC cells.

Immunofluorescent analysis

NSCLC cells were inoculated in 6-well dishes and allowed to adhere for 1 day. After treating with Raddeanin A at indicated concentrations (0, 1, 2, 4 μM) for 24 h, 1 mL of 1 % BSA was added to the plate, which was incubated for 40 min to provide confinement, and 4 % PFA was added to each well to fix the cells. 0.1 % TritonX-100 was added to the cells and incubated for 30 min to permeabilize the cells. Containment was provided by the addition of 10 % goat serum and incubation in a water bath at 37°C for 1 h. Specific primary antibodies were applied at room temperature overnight. The following day, the cells were washed and then incubated with fluorescein-labeled goat anti-rabbit IgG antibody for 2 h at room temperature away from light. The nuclei were counterstained with DAPI, and the cells were observed under an Olympus fluorescence microscope at room temperature. Tissue samples were processed for immunofluorescence analyses in a similar manner. Images were processed using ImageJ software.

Plasmid transfection

CDK6 overexpression was performed with the CDK6 cDNA plasmid (GV657 CMV enhancer-MCS-3flag-polyA-EF1A-zsGreen-sv40-puromycin; Shanghai Gene Chem). Transfection was performed using Lipofectamine 3000 (Invitrogen, Carlsbad, CA, USA) and P 3000 according to the manufacturer's instructions. After 6 h, 10 % FBS RPMI-DMEM medium was added to the cells in the treatment group for 48 h.

Network pharmacological analysis

Possible drug targets can be predicted by comparing the chemical structures and molecular shapes of novel drugs to those of established drugs [26,27]. Here, DrugBand, Genecard, TTD, OMIM, Swiss, PharmMapper and PharmGkb database were used to predict potential disease-related drug targets, and the resulting targets were compared to possible targets of drugs analyzed here as identified with Swiss Target Prediction. Import the intersecting targets into the STRING database to construct a protein-protein interaction (PPI) network, and then use Cytoscape software for network visualization and core gene identification (CytoNCA). Additionally, perform clustering analysis using the MCODE plugin in Cytoscape to construct highly connected sub-networks and select core targets of Raddeanin A against NSCLC. Finally, conduct GO and KEGG enrichment analyses to gain deeper insights into the functions of the screened genes and identify several potential targets.

Molecular docking and molecular dynamics simulation

Select the target protein of the highest-scoring cluster (cluster1) from the clustering analysis using the MCODE plugin in Cytoscape. Obtain the 3D structure of the protein from the AlphaFold Protein Structure Database (https://alphafold.ebi.ac.uk/) to use as the receptor. Download the 3D structure of Raddeanin A from the PubChem database (https://pubchem.ncbi.nlm.nih.gov/). Use the CB-Dock2 website to perform preprocessing of the molecule, including removing water and adding hydrogen atoms, setting the active pocket, and exporting the data in gpf format. Conduct molecular docking validation using the CB-Dock2 website, export the results in pdb format, and visualize them in PyMol 2.6.0.

Using GROMACS 2020.3 software, a 100 ns molecular dynamics (MD) simulation was conducted to further validate the docking results' rationality and reliability. The OPLS-AA/L all-atom force field and the Amber GAFF force field were utilized to generate parameters and topology files for the protein and the small molecule ligand, respectively. Periodic boundary conditions were set and optimized to simulate the size of the constraint box, filling the box with water molecules. To ensure the system's electrical neutrality, some solvent water molecules were replaced with Na+ and Cl- at a concentration of 0.15 mol/L. The steepest descent method was used to minimize the entire system's energy. Pre-equilibration was conducted in two stages: the first stage used the NVT ensemble at 300 K and 100 ps to stabilize the system's temperature, and the second stage used the NPT ensemble at 1 bar and 100 ps to stabilize the system's pressure. This was followed by molecular docking and molecular dynamics simulations.

Molecular simulation and molecular docking techniques were used to identify potential drug targets the mechanisms of their interactions. High-resolution X-ray crystal structures of human CDK6 proteins were identified from the PDB database, and these structures were used to determine the site of interaction and the binding energy between the protein and Raddeanin A. The stability of the interaction between the natural product and the protein was assessed with molecular dynamics simulations.

Surface plasmon resonance (SPR) analysis

SPR was used to quantify the affinity between CDK6 and Raddeanin A. CDK6 (50 μg/mL) was diluted in fixation buffer (10 mM sodium acetate, pH 4.0). Next, 400 mM 1-ethyl-3-(3-dimethyl. aminopropyl) carbodiimide was mixed with 100 mM N-hydroxysuccinimide to prepare the activator. After activation of the s-series CM5 sensor chip, the protein sample was injected into the FC3 sample channel at a flow rate of 10 μL/min for 420 s. The chip was deactivated by adding a solution of 1 M ethanolamine hydrochloride-NaOH (GE) at a flow rate of 10 μL/min for 420 s. Raddeanin A was diluted in same run buffer (PBST, PH7.4;1 % DMSO PBST, PH7.4) to a series of concentrations between 0 and 15.6 μM and then injected into Fc1(reference channel)-Fc3(sample channel) channels at a flow rate of 30 μL/min for 120 s to achieve the association phase, and then buffer was administered for 300 s to establish the dissociation phase. The data were processed and analyzed using Biacore 4000 and Biacore T200 evaluation software (GE Healthcare).

Co-immunoprecipitation assay

Magnetic protein A/G agarose beads were obtained from Beyotime Biotechnology. The beads were washed with PBS and incubated with 5 % BSA in a four-dimensional rotating mixer at 4°C for 2 h. Solutions of proteins extracted from treated cells or tissues were pre-cleared with magnetic beads, and then primary antibodies were added to the supernatant, and the samples were incubated overnight in a four-dimensional rotating mixer at 4°C. The next day, magnetic beads were added, and the samples were incubated for 2 h in a four-dimensional rotating mixer at 4°C. The lower precipitate was washed with PBS and specific immunoprecipitated proteins were separated by SDS-PAGE.

Animal studies

Female BALB/c nude mice (6–8 weeks old) were used throughout the study. Matrigel was diluted 1:1 and then added to 5×10^6 A549 cells, with a total volume of 100 μL. These samples cells were then injected subcutaneously into nude mice aged 6 to 8 weeks. Approximately 1 week later, when the tumor volume was at least 50 mm^3, the mice were divided randomly into four groups ($n = 7$) that were treated as follows: vehicle control, abemaciclib (10 mg/kg), Raddeanin A (0.5 mg/kg) and Raddeanin A (1.0 mg/kg), were intraperitoneally injected once every 2 days starting on day 18 for 7 times for 30 days. The mice in each group were treated on alternate days for a total of 7 treatments. There was no significant change in body weight during the experiment. The mice were sacrificed 4 h after the last dose. Tumors, hearts, livers, kidneys and lungs were extracted from mice of each group for histological staining and Western blotting analyses.

Statistical analysis

Each experiment was performed in triplicate. The results are represented as means ± SD, and SPSS21.0 was employed for performing statistical analyses. Multiple groups were compared with one-way ANOVA and Tukey's tests. Differences were considered statistically significant when $p < 0.05$.

Results

Raddeanin A treatment lowers NSCLC cell viability

The effect of Raddeanin A on the proliferative capacity of NSCLC cells was investigated using the MTT assay (Fig. 1). The proliferation of all tested NSCLC cell lines (H1299, A549, PC-9, HCC827 and H1975) was inhibited by Raddeanin A in a dose- and time-dependent manner, with IC_{50} values between 1 and 4 μM. Conversely, the inhibitory effect of Raddeanin A on the proliferation of the normal human bronchial epithelium cell line BEAS-2B was weaker, with an IC_{50} value of 9.480 ± 1.091 μM. This is nearly ten times higher than the IC_{50} of NSCLC cells (Fig. 1B and Supplementary Fig. 1A). Colony formation experiments also showed that Raddeanin A-treated NSCLC cell lines had significantly reduced proliferative capacity compared with the control group, suggesting that Raddeanin A has the ability to inhibit the formation of NSCLC clones. Importantly, Raddeanin A only exhibited a weak inhibitory effect on the clonal formation of BEAS-2B cells (Fig. 1C). Similarly, in the EdU assay, Raddeanin A decreased the percentage of NSCLC cells staining positive for EdU incorporation (Fig. 1D), further supporting the decrease of viability upon Raddeanin A treatment.

Raddeanin A inhibits NSCLC cell migration and invasion

The effects of Raddeanin A on the migration and invasion ability of NSCLC cells in vitro were investigated using wound healing and transwell assays (Fig. 2). As shown in Fig. 2A and B, we observed a dose-dependent decrease in the migratory ability of NSCLC cells after 24 h of treatment with Raddeanin A. Raddeanin A was also found to significantly reduce the invasive ability of NSCLC cells (Fig. 2D).To investigate the mechanism by which Raddeanin A treatment inhibited the migration of NSCLC cells, Western blotting was used to quantify the effects of Raddeanin A treatment on the expression of several proteins involved in cell migration: E-cadherin, vimentin, Snail and MMP2. After Raddeanin A treatment of PC-9, A549 and H1299 cells, the levels of E-cadherin were found to be increased, while the levels of vimentin, Snail and MMP2 were found to be decreased (Fig. 2D and Supplementary Fig. 1B).

Raddeanin A causes G1 phase arrest in NSCLC cells

We first identified potential drug targets in NSCLC through analyses of the DrugBand, Genecard, TTD, OMIM, and PharmGkb databases (Fig. 3A). Then, the Swiss target prediction database was used to predict possible targets of Raddeanin A; the list of these possible targets was compared with the list of possible disease targets to obtain overlapping Raddeanin A targets of potential interest in NSCLC (Fig. 3B). Import the intersecting targets of drugs and diseases into the STRING database to construct a protein-protein interaction (PPI) network, followed by network visualization using Cytoscape(Fig. 3C).Additionally, perform clustering analysis with the MCODE plugin in Cytoscape to build highly connected subnetworks and categorize the targets into seven classes. Select the highest-scoring cluster, Cluster 1, and perform GO and KEGG enrichment analyses on the list of core genes. The KEGG enrichment analysis indicated that Raddeanin A is a potential drug for treating NSCLC (Supplementary Fig. 2A). In particular, the GO enrichment analysis suggested that Raddeanin A may exert anticancer effects through targeting CDKs (Supplementary Fig. 2B). Then perform molecular docking simulations of the gene targets within this cluster with Raddeanin A (Fig. 3D).The results of molecular docking are represented by binding energy, which indicates the binding activity between the receptor and the ligand. When the binding energy is <0 kJ/mol, it can be determined that the ligand and receptor have the ability to bind spontaneously. The smaller the binding energy, the higher the affinity between the receptor and the ligand, and the greater the likelihood of interaction. According to the data in the table, the 39 docked proteins were ranked by binding free energy, identifying the top 10 key proteins: IGF1R, ATM, ERBB2, MET, IL10, TERT, MCL1, CDK4, MDM2, and CDK6. These targets have the closest binding with the ligand (Fig. 3E).

Because the network pharmacology analyses suggested that Raddeanin A treatment may affect proteins involved in the cell cycle (Supplementary Fig.2B), we conducted cell flow cytometry experiments to analyze the effect of Raddeanin A treatment on cell cycle progression. When H1299, A549 and PC-9 cells were treated with Raddeanin A at concentrations of 0, 1, 2 and 4 μM for 24 h, Raddeanin A was found to increase the percentage of cells in G1 phase in a dose-dependent manner (Fig. 3F). According to Western blot analyses, the expression of CDK6 was decreased in these cell types upon treatment with Raddeanin A, and a corresponding decrease in the phosphorylation of Rb was also observed. The levels of CDK4 and cyclin D1 were unchanged, suggesting that Raddeanin A may have a selective inhibitory effect on CDK6 (Fig. 3G and Supplementary Fig. 2C).

Raddeanin A targets CDK6 in NSCLC

The results of the cell cycle analyses led us to hypothesize that CDK6 is a potential direct target of Raddeanin A, which directly inhibits the expression of CDK6 protein. In agreement with this prediction, molecular docking simulations using high resolution X-ray crystal structures of human CDK6 identified a potential direct interaction between Raddeanin A and CDK6 (Fig. 4A). We performed molecular dynamics simulations on the molecular docking results. As shown in the figure, the RMSD values initially fluctuated gradually and eventually stabilized around 0.6. The binding energy stabilized between 40–100 ns, ultimately maintaining at −60. Molecular fluctuations also stabilized within the

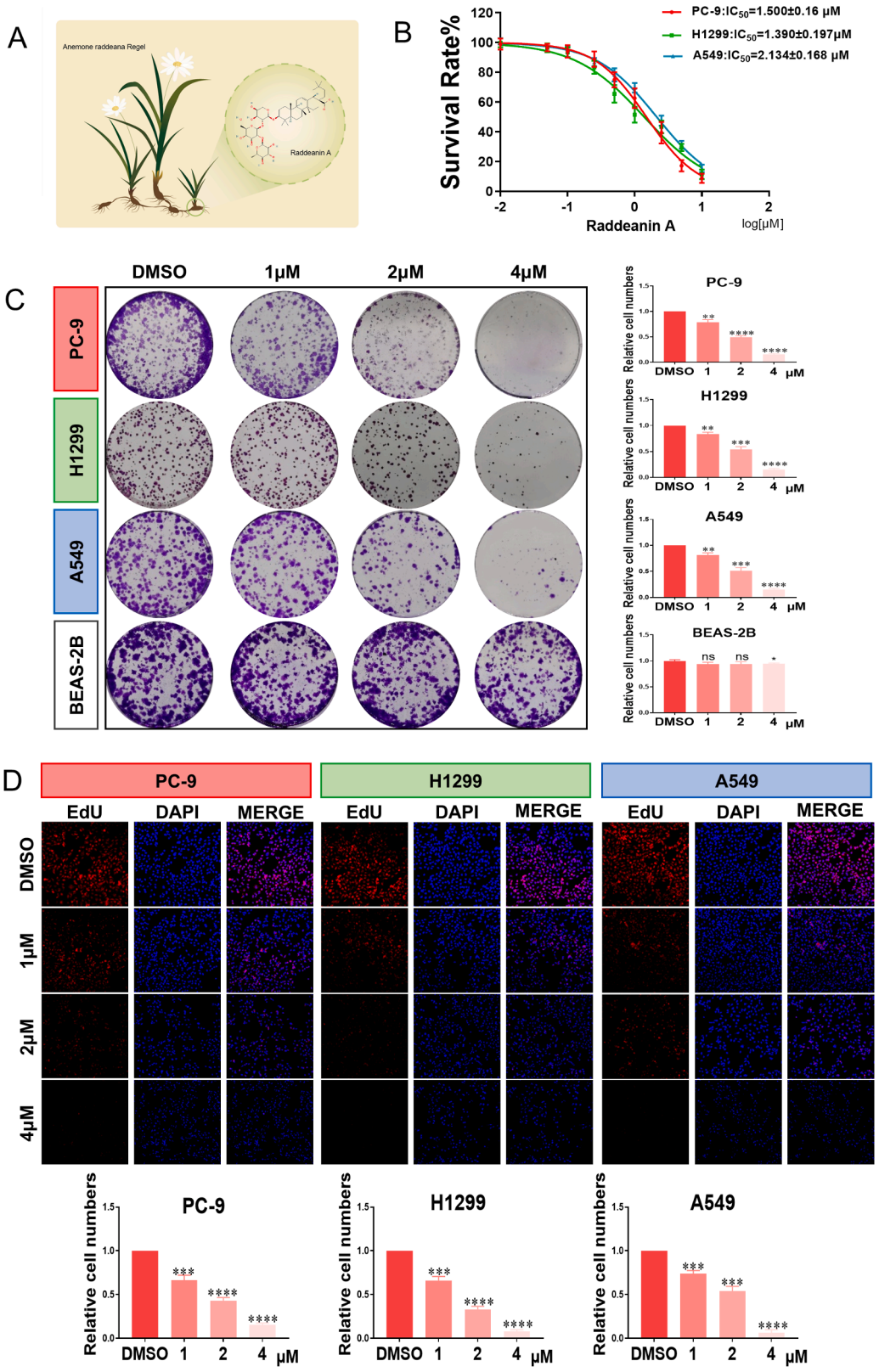

Fig. 1. *Raddeanin A inhibits NSCLC cell viability.* (A) The chemical structural formula of Raddeanin A. (B) Detection of IC_{50} values of NSCLC cells. (C) Detection of colony forming ability of NSCLC cell lines. (D) Observation of cell proliferation using EdU. Attention should be paid to the number of EdU positive cells Scale bar=200 μM. $^{*}P < 0.05$, $^{**}P < 0.01$, $^{***}P < 0.001$, $^{****}P < 0.0001$.

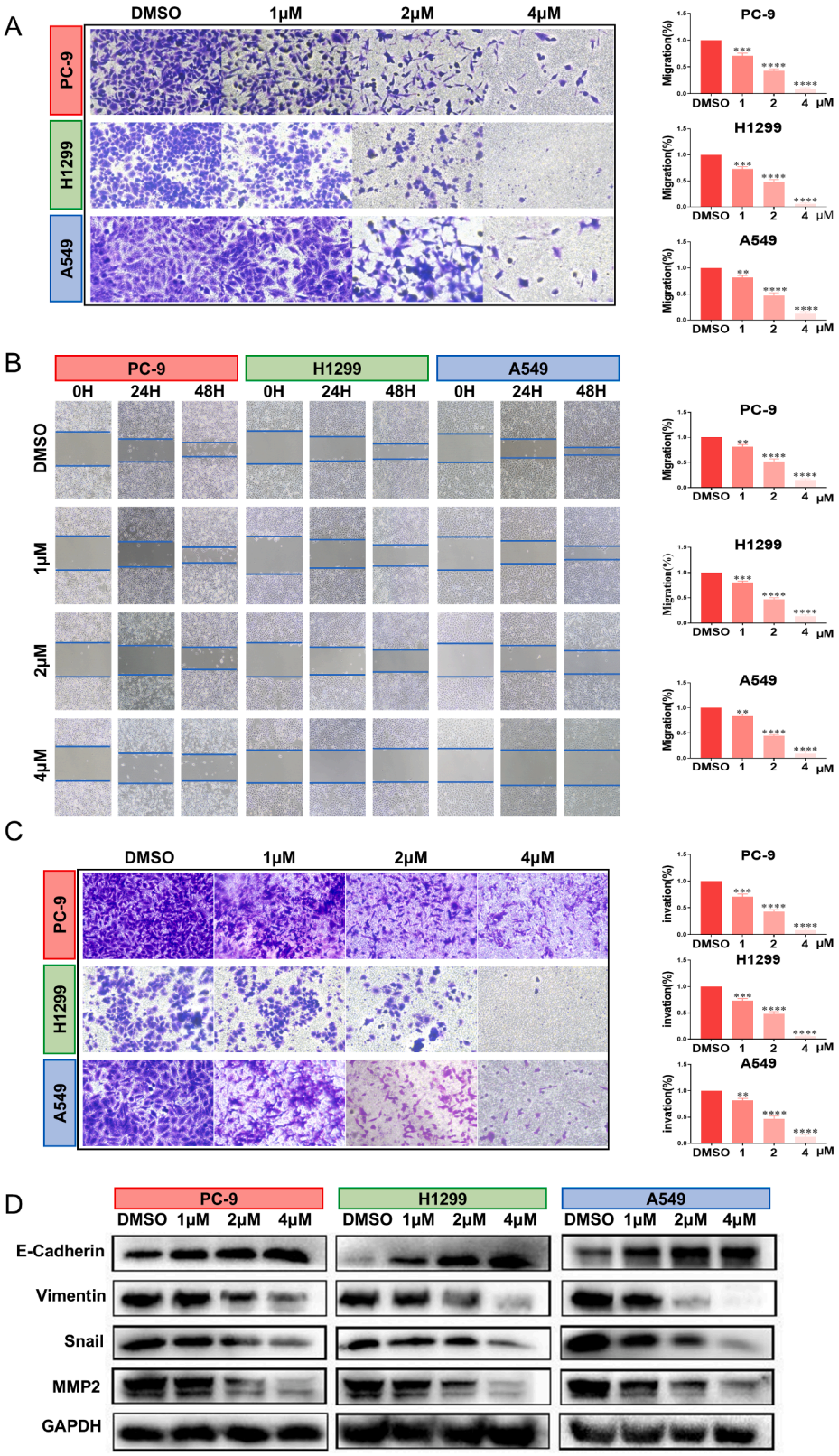

Fig. 2. *Raddeanin A inhibits NSCLC cell migration and invasion.* (A, B) Raddeanin A (0,1,2 and 4 μM) was assayed for its effect on the migratory ability of the three NSCLC cells lines. The transwell assay and the scratch assay of the three NSCLC cells lines. (C) Transwell invasive assay to detect the invasive ability of three NSCLC cell lines. Scale bar=100 μM. $^{*}P < 0.05$, $^{**}P < 0.01$, $^{***}P < 0.001$, $^{****}P < 0.0001$. (D) Detection of protein expression levels of E-cadherin, Vimentin, Snail and MMP2 in three NSCLC cell lines after 24 h by Western blotting.

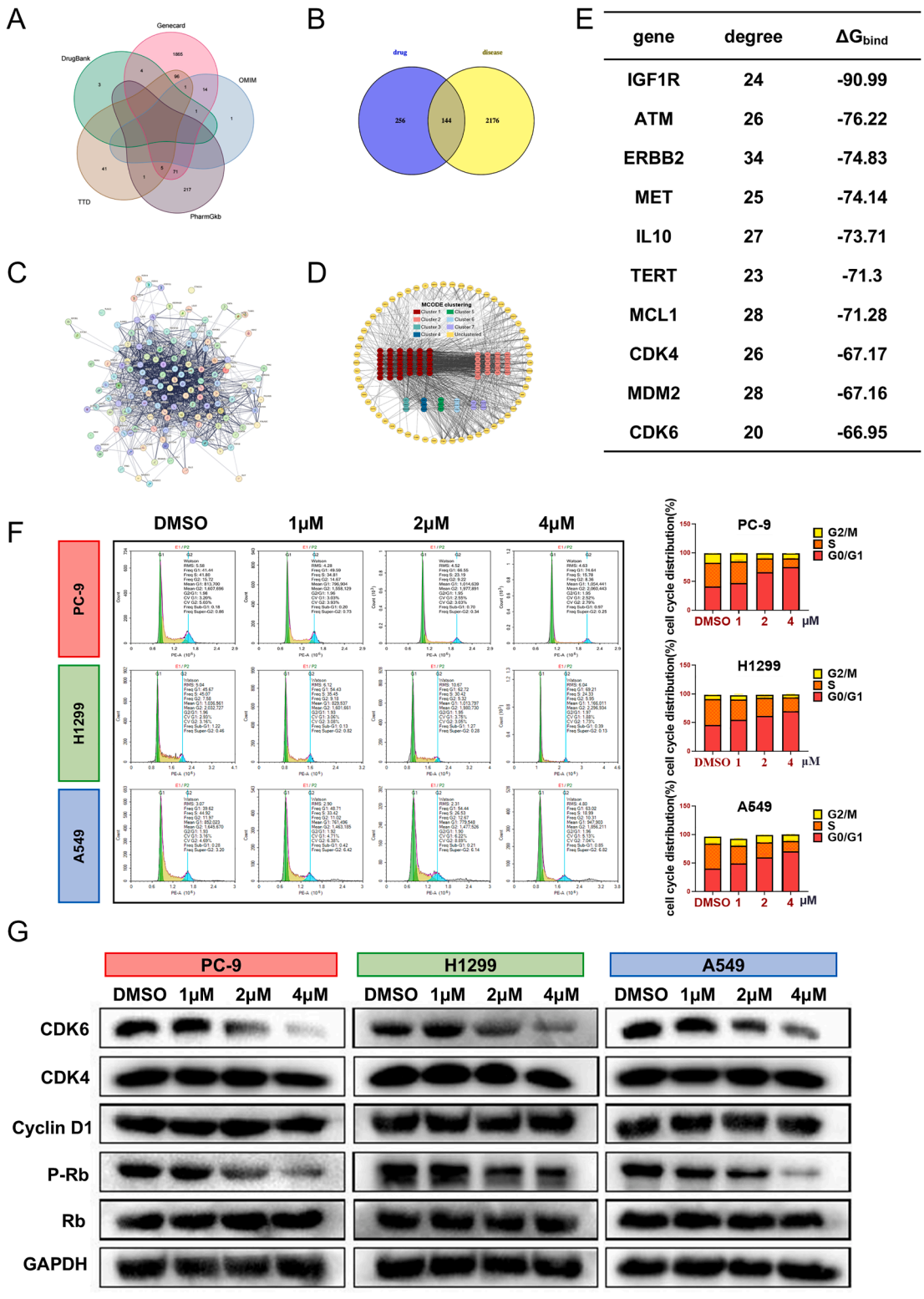

gene	degree	ΔG_{bind}
IGF1R	24	-90.99
ATM	26	-76.22
ERBB2	34	-74.83
MET	25	-74.14
IL10	27	-73.71
TERT	23	-71.3
MCL1	28	-71.28
CDK4	26	-67.17
MDM2	28	-67.16
CDK6	20	-66.95

Fig. 3. *Raddeanin A causes G1 phase arrest of NSCLC cell cycle.* (A) All possible targets for NSCLC were identified through the DrugBand, Genecard, TTD, OMIM, and PharmaGkb databases. (B) Using Cytoscape software to construct the core of the PPI network (CytoNCA) and search for core genes. (C) The PPI network core (CytoNCA) was constructed using Cytoscape software to search for core genes. (D) Use the MCODE plugin in Cytoscape to conduct clustering analysis, constructing highly connected subnetworks and classifying the targets into seven categories. (E) molecular docking simulations of the gene targets. (F) Flow cytometry experiments were performed to detect the proportion of cells stalled in G1 phase in the three NSCLC cell lines treated with Raddeanin A (0,1, 2 and 4 μM). (G) Use Western blotting to detect the expression levels of CDK4, CDK6, Rb, and P-Rb in the three NSCLC cell lines.

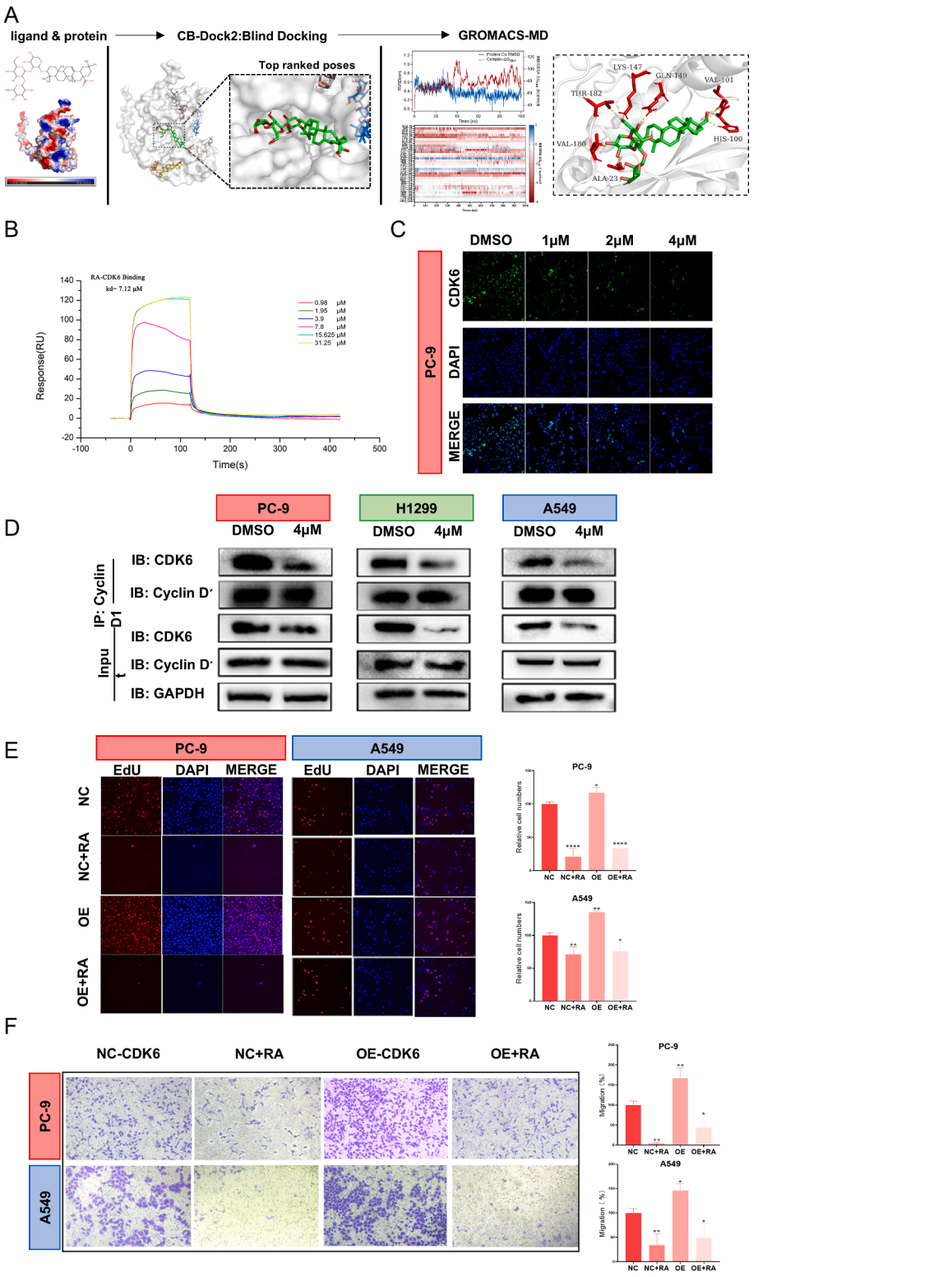

Fig. 4. *Raddeanin A targets CDK6 in NSCLC.* (A) Using molecular docking simulation, the amino acid sites of Raddeanin A interacting with CDK6 are displayed. (B) The direct binding effect between CDK6 and Raddeanin A was verified through SPR experiments, with an affinity of 7.12 μM for CDK6. (C) Immunofluorescence assays were used to detect changes in fluorescence levels of the three NSCLC cell lines examined after treatment with Raddeanin A (4 μM) for 24 h. CDK6 immunofluorescence staining (green) and nuclear staining (blue). Scale bar=200 μM. $^{*}P < 0.05$, $^{**}P < 0.01$, $^{***}P < 0.001$, $^{****}P < 0.0001$. (D)The expression levels of CDK6 and cell cycle protein D1 in the three NSCLC cell lines after treatment with Raddeanin A (4 μM) for 24 h were detected using the Co-IP assay. (E) The cell proliferation of NSCLC cell lines after CDK6 overexpression and drug treatment was detected, and the cell proliferation was observed by EdU. Note that EdU positive cell count scale =200 μM. $P < 0.05$, $^{**}P < 0.01$, $^{***}P < 0.001$, $^{****}P < 0.0001$. (F) The effects of Raddeanin A (2 μM) treatment after CDK6 overexpression and after CDK6 overexpression on the migration ability of two NSCLC cell lines were examined. The migration abilities were evaluated by performing transwell assays on these two NSCLC cell lines.

40–100 ns interval, indicating a tight binding between the protein and the ligand, facilitated by specific hydrogen bonds at the binding sites including VAL-101, HIS-100, GLN-149, LYS-147, THR-182, VAL-180, and ALA-23 (Fig. 4A). Accordingly, SPR spectroscopy using recombinant human CDK6 demonstrated direct binding between CDK6 and Raddeanin A, with an affinity of 7.12 μM, which is of the same order of magnitude and relatively close to the IC_{50} of NSCLC. (Fig. 4B). Initial immunofluorescence imaging revealed that CDK6 was predominantly localized in the cytoplasm of untreated cells (Fig. 4C). Notably, upon treatment with Raddeanin A, we observed a dose-dependent decrease in CDK6-specific fluorescence intensity, indicating that Raddeanin A may destabilize the CDK6 protein (Fig. 4C).

Of the many protein interactions that are involved in the regulation of G1 phase of the cell cycle [28], one of the most important is the pathway in which cyclin D1 binding activates the kinase activity of CDK4/6 to phosphorylate Rb. Importantly, we found by immunoprecipitation analysis that Raddeanin A reduced CDK6 binding to cell cycle protein D1 by reducing CDK6 expression (Fig. 4D and Supplementary Fig. 3A), this disruption of the CDK6/cyclin D1 complex would be expected to prevent the cells from transitioning from G1 to S phase.

To further confirm CDK6 as a target in Raddeanin A, we conducted experiments by transfecting both control plasmids and plasmids overexpressing CDK6 into PC-9 and A549 cells. Upon confirming the successful overexpression of CDK6, we then proceeded to conduct EdU staining (Fig. 4E). This experiment demonstrated a significant enhancement in cellular proliferation ability following CDK6 overexpression. Additionally, Transwell and wound healing assays further confirmed that CDK6 overexpression led to an increase in cellular migration capacity (Fig. 4F and Supplementary Fig. 3B). However, when we treated PC-9 and A549 cells overexpressing CDK6 with 2 μm Raddeanin A, we found that the migration and proliferation abilities of these cells were suppressed compared to the overexpression group. These findings suggest that Raddeanin A may exert its antitumor effects by inhibiting CDK6 function in NSCLC cells.

Raddeanin A inhibits the proliferation of NSCLC in vivo

The anti-tumor effect of Raddeanin A was studied in nude mice following subcutaneous injection of A549 cells. The tumor-bearing mice were randomly assigned to four treatment groups ($n = 7$). Mice in these groups were treated with vehicle control, 0.5 mg/kg Raddeanin A, 1 mg/kg Raddeanin A or 10 mg/kg abemaciclib (a known CDK4/6 inhibitor). The volumes and weights of tumors of mice treated with 0.5 mg/kg Raddeanin A or with abemaciclib were slightly reduced relative to control. However, intraperitoneal injection of 1 mg/kg Raddeanin A significantly reduced tumor volume and weight (Fig. 5A–C). These impacts on tumor growth were mirrored by decreased expression of CDK6 and decreased phosphorylation of Rb, as determined by Western blotting of proteins extracted from tumor tissues (Fig. 5E) and by immunohistochemical analyses (Fig. 5D). The body weights of the mice were not significantly changed in any treatment group (Fig. 5F). In addition, no significant toxicity of the injected drug was identified by histochemical staining of heart, liver, lung and kidney tissues from the treated mice (Fig. 5G).

Discussion

Lung cancer is one of the leading causes of oncogenic mortality [29]. A broad approach to modern cancer treatment is to identify a single oncogenic driver gene [30]. An important hallmark of cancer is cell cycle imbalance due to the abnormal activation of CDKs [31]. The G1 restriction point is critical for regulating the cell cycle and is controlled by the retinoblastoma pathway, which involves cyclin D1 and CDK 4/6 [32]. Accordingly, CDK4/6 inhibitors inhibit the progression of tumor cells sensitive to them from the G1 to the S phase of the cell cycle. The use of CDK4/6 inhibitors to treat NSCLC has been found to be relatively safe, allowing continuous administration to achieve sustained target inhibition [33]. Thus, the identification of additional CDK4/6 inhibitors would be an important step in the development of more effective treatments for NSCLC.

At present, several clinical trials of CDK4/6 inhibitors in a variety of tumors are currently showing promising preliminary results, such as breast cancer [34] and lung cancer [35]. Whether CDK4/6 inhibitors can be promising broad-spectrum antitumor agents and how their clinical effects can be maximized remains uncertain [9]. A variety of potent CDK4/6 inhibitors are currently used in clinical practice and are considered relatively safe, but several important adverse effects have been identified, including fatigue and toxicity to the gastrointestinal tract, kidneys, and hematopoietic system [33]. Therefore, the identification of new effective and safe CDK4/6 inhibitors would have an important impact on the treatment of NSCLC. In the present study, Raddeanin A, a natural triterpenoid saponin from *Rhizoma aconiti,* performed better than a CDK4/6 inhibitor used in clinical practice in terms of dosage and efficacy. Therefore, Raddeanin A is a potential traditional Chinese medicine component with clinical medication potential.

Plant extracts represent natural chemicals that can be used to treat various diseases; in particular, they have been found to be associated with significant anticancer effects. Accordingly, the potential of low-toxicity plant-derived natural compounds for pharmaceutical use is a key research goal. In this study, we propose for the first time that Raddeanin A causes cell cycle arrest in NSCLC cells in vitro and in vivo by targeting CDK6. Specifically, we demonstrated that Raddeanin A can reduce the proliferation of NSCLC cells (Fig. 1), inhibit NSCLC cell migration and invasion (Fig. 2), inhibit the CDK6 pathway (Figs. 3 and 4) and induce cell cycle arrest (Fig. 3). In addition, mice treated with Raddeanin A exhibited strong tumor growth inhibitory effects (Fig. 5). Thus, Raddeanin A is a natural herbal monomer with significant antitumor effects (Fig. 6).

Raddeanin A is known to inhibit CDK6 expression levels and has been shown to have strong anti-angiogenic and anti-tumor activity. Only a few studies have reported the adverse effects of Raddeanin A, although further research is needed to evaluate its toxicity [36]. Overall, however, studies into the pharmacology of Raddeanin A are not yet comprehensive, and further research is needed to optimize its clinical use.

In summary, Raddeanin A has demonstrated significant anti-NSCLC effects both in vitro and in vivo. The potential mechanism of Raddeanin A's anti-NSCLC activity may involve inhibiting CDK6, thereby disrupting the formation of its complex with cyclin D1, which blocks the progression of the cell cycle from the G1 phase to the S phase, thus exerting its anti-NSCLC effects without noticeable toxic side effects. Therefore, Raddeanin A has the potential to become a highly promising CDK6 inhibitor for NSCLC in clinical settings. However, whether this natural compound can produce substantial clinical benefits requires further clinical evaluation in future studies.

Despite these promising findings, several limitations of this study should be acknowledged. First, our in vivo validation was exclusively performed in immunodeficient A549 xenograft models, which cannot fully recapitulate the tumor microenvironment (e.g., immune cell interactions) or molecular heterogeneity observed in human NSCLC. Second, while Raddeanin A demonstrated efficacy across multiple adenocarcinoma cell lines (A549, H1975, PC-9), its effects on squamous cell carcinoma remain unexplored, limiting the generalizability of our conclusions. Third, although minimal cytotoxicity was observed in BEAS-2B normal lung epithelial cells, comprehensive safety profiling in vivo and systematic analysis of other critical pathways (e.g., apoptosis regulators, DNA damage response) in normal cells were not conducted. Finally, as a natural product, Raddeanin A may engage additional targets beyond CDK6, and our study did not employ global proteomic approaches (e.g., kinome screening or chemoproteomics) to map its full interactome—an essential step for understanding potential off-target effects.

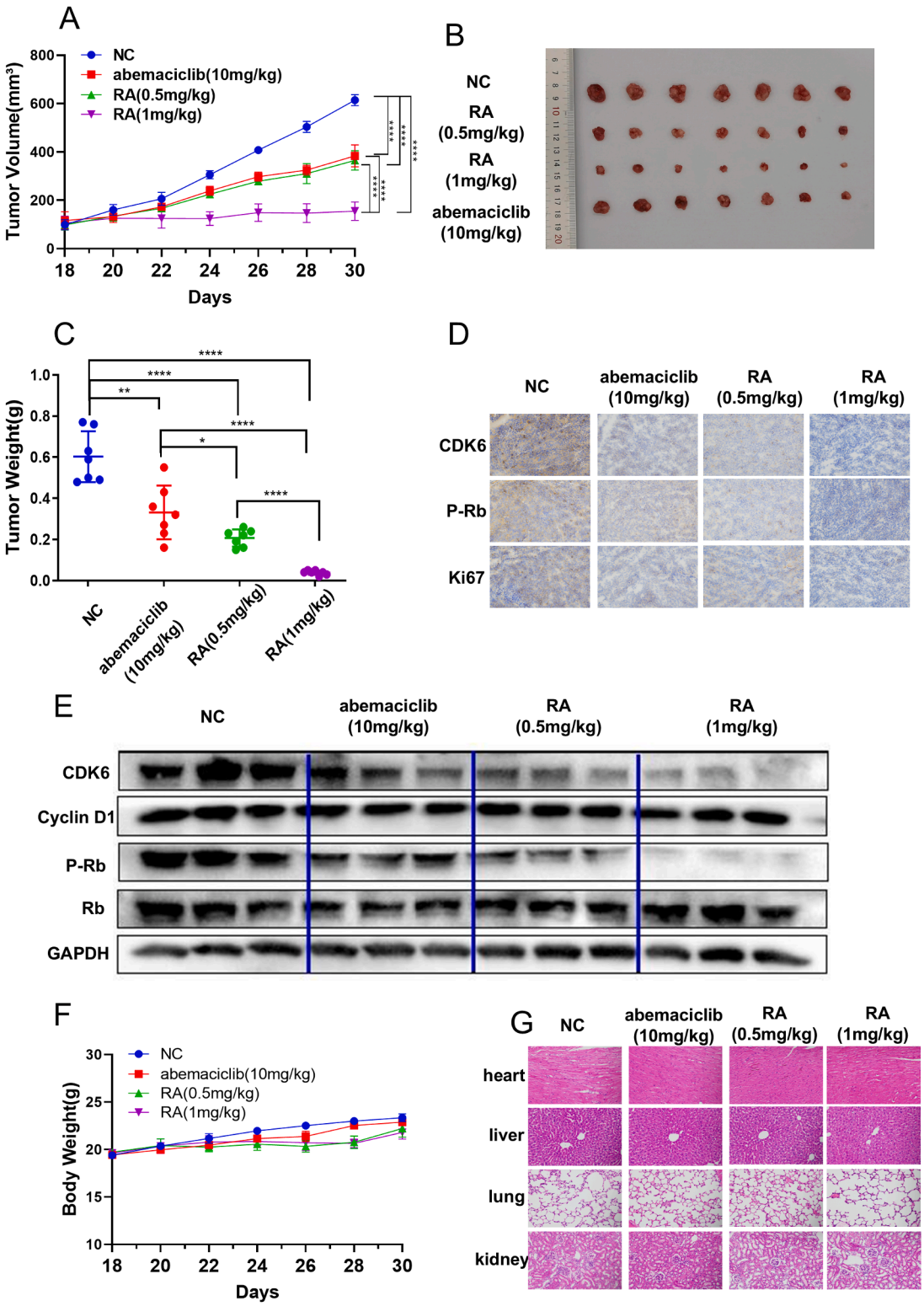

Fig. 5. *Raddeanin A inhibits the proliferation of NSCLC* in vivo. (A) Mouse tumor size growth curve. Nude mice were divided into control group, 0.5 mg/kg group, 1 mg/kg group, and CDK4/6 inhibitor group (abemaciciclib group). Record the tumor volume every 2 days and weigh the mice. (B) Representative images of tumor tissue ($n = 7$). (C) Measurement of tumor weight. (D) The expression levels of Ki67, CDK6, and P-Rb were tested using IHC staining.(E) Protein levels of CDK4, CDK6 and CyclinD1 as well as total and phosphorylated protein levels of Rb were examined by Western blotting. Scale bar=100 μM. (F) Mouse body weight curve. (G) The hematoxylin and eosin staining of the heart, liver, lungs, and kidneys did not show histological abnormalities. *$P < 0.05$, **$P < 0.01$, ***$P < 0.001$, ****$P < 0.0001$.

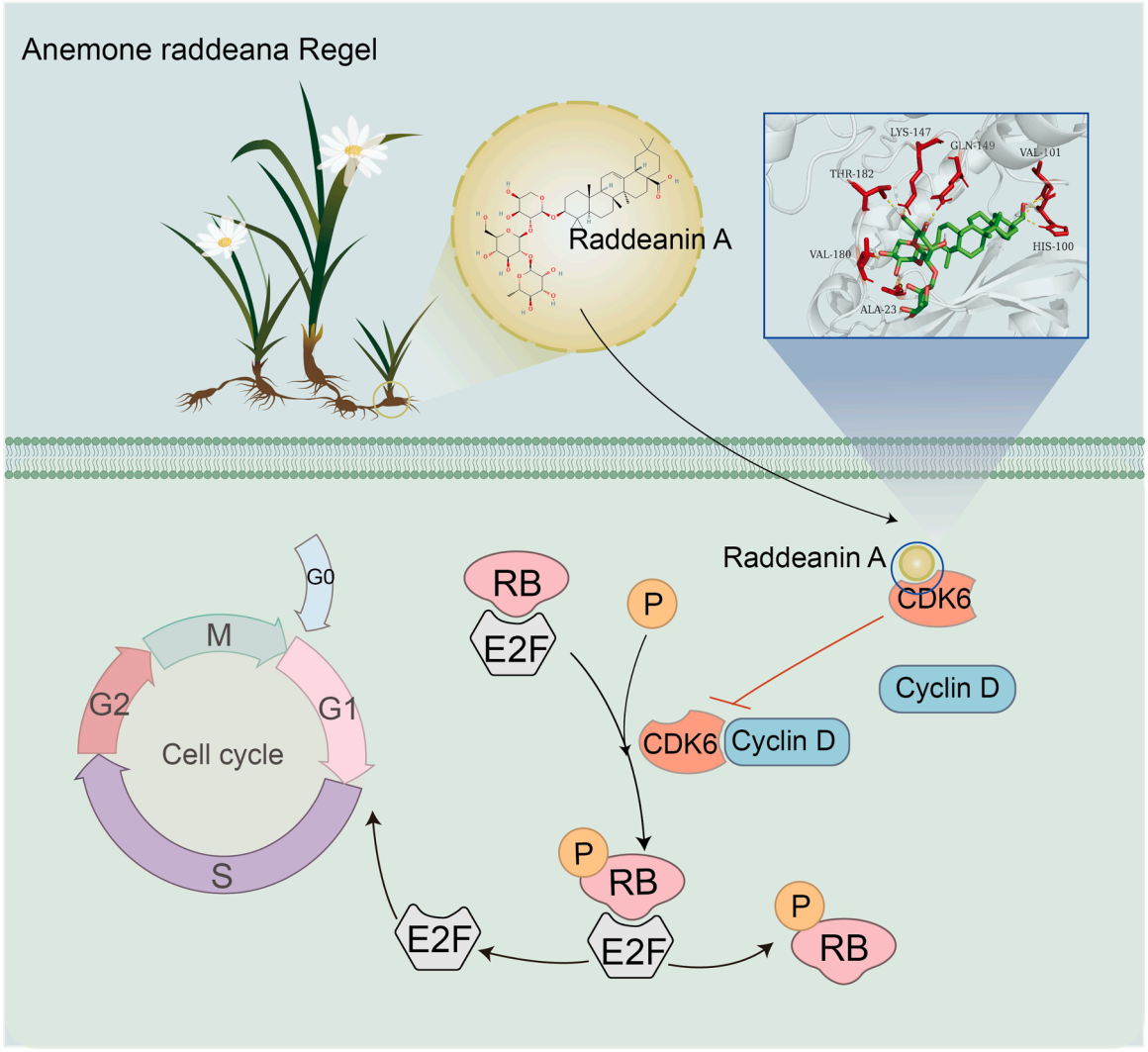

Fig. 6. Mechanism diagram of Raddeanin A anti NSCLC cells.

Future studies should address these gaps by: (1) employing patient-derived xenografts (PDXs) or immunocompetent models to evaluate tumor-immune crosstalk; (2) validating efficacy in squamous cell carcinoma models (e.g., NCI-H1703) and EGFR/KRAS co-mutant NSCLC subtypes; (3) conducting GLP-compliant toxicity assessments across major organ systems; and (4) integrating multi-omics strategies to systematically characterize Raddeanin A's polypharmacology.

Conclusions

Our findings demonstrate that Raddeanin A exhibits potent CDK6 inhibitory activity in NSCLC cells, suggesting its potential as a novel therapeutic candidate. However, the ability of this herbal monomer to produce substantial clinical benefit needs to be clinically evaluated in NSCLC patients in future studies. These investigations into the activity of Raddeanin A provide avenues for exploring new CDK4/6 inhibitors.

CRediT authorship contribution statement

Xian Wang: Writing – original draft. **Xiao Lin:** Writing – review & editing, Visualization, Formal analysis. **Yuxin Liu:** Conceptualization. **Chunbo Ma:** Methodology, Investigation. **Mengchu Liu:** Funding acquisition. **Jiayu Bai:** Project administration. **Yihan Ye:** Validation, Software. **Chengguang Zhao:** Project administration, Methodology, Investigation. **Lehe Yang:** Data curation, Conceptualization. **Xiaoying Huang:** Funding acquisition, Formal analysis. **Liangxing Wang:** Visualization, Validation, Supervision.

Declaration of competing interest

All authors have no potential conflicts of interest to disclose.

Ethics approval

The animal experiments procedures were performed following the International Laboratory Animal Care guidelines. The animal experiment protocols were approved by the Animal Care and Use Committee of Wenzhou Medical College.

Acknowledgments

This work was financially supported by the National Natural Science Funding of China (82203322 and 82173856), Natural Science Foundation of Zhejiang Province (LY24H160029), Collaborative Education Project of Industry, University and Research Cooperation of the Ministry of Education (220604408242859), Wenzhou Science and Technology Project (H20210009 and Y20220037), Special funding of Discipline Cluster of Oncology, Wenzhou Medical University, China (z2-2023017).

Consent for publication

All authors have agreed to publish this manuscript.

Availability of data and material

The data set used and analyzed in this article would be available from the corresponding author on request.

Supplementary materials

Supplementary material associated with this article can be found, in the online version, at doi:10.1016/j.tranon.2025.102382.

References

[1] D. Miao, J. Zhao, Y. Han, J. Zhou, X. Li, T. Zhang, et al., Management of locally advanced non-small cell lung cancer: state of the art and future directions, Cancer Commun. (Lond) 44 (2023) 23–46, https://doi.org/10.1002/cac2.12505.

[2] T.V. Denisenko, I.N. Budkevich, B. Zhivotovsky, Cell death-based treatment of lung adenocarcinoma, Cell Death. Dis. 9 (2018) 117, https://doi.org/10.1038/s41419-017-0063-y.

[3] Y. Tang, Y. Wang, X. Wang, Z. Zhao, H. Cai, M. Xie, et al., Acetylshikonin exerts anti-tumor effects on non-small cell lung cancer through dual inhibition of STAT3 and EGFR, Phytomedicine 101 (2022) 154109, https://doi.org/10.1016/j.phymed.2022.154109.

[4] D.O. Morgan, CYCLIN-DEPENDENT KINASES: engines, clocks, and microprocessors, Annu. Rev. Cell Dev. Biol. 13 (1997) 261–291, https://doi.org/10.1146/annurev.cellbio.13.1.261.

[5] S. Lim, K.P. Cdks, cyclins and CKIs: roles beyond cell cycle regulation, Development 140 (15) (2013) 3079–3093, https://doi.org/10.1242/dev.091744.

[6] M. Malumbres, M. Barbacid, Mammalian cyclin-dependent kinases, Trends. Biochem. Sci. 30 (11) (2005) 630–641, https://doi.org/10.1016/j.tibs.2005.09.005.

[7] B. O'Leary, R.S. Finn, N.C. Turner, Treating cancer with selective CDK4/6 inhibitors, Nat. Rev. Clin. Oncol. 13 (7) (2016) 417–430, https://doi.org/10.1038/nrclinonc.2016.26.

[8] C.J. Sherr, D. Beach, G.I. Shapiro, Targeting CDK4 and CDK6: from discovery to therapy, Cancer Discov. 6 (2016) 353–367, https://doi.org/10.1158/2159-8290.CD-15-0894.

[9] Q. Du, X. Guo, M. Wang, Y. Li, X. Sun, Q. Li, The application and prospect of CDK4/6 inhibitors in malignant solid tumors, J. Hematol. Oncol. 13 (2020) 41, https://doi.org/10.1186/s13045-020-00880-8.

[10] C. Yang, C.A. Boyson, M. Di Liberto, X. Huang, J. Hannah, D.C. Dorn, et al., CDK4/6 inhibitor PD 0332991 sensitizes acute myeloid leukemia to cytarabine-mediated cytotoxicity, Cancer Res. 75 (2015) 1838–1845, https://doi.org/10.1158/0008-5472.CAN-14-2486.

[11] N.C. Turner, J. Ro, F. André, S. Loi, S. Verma, H. Iwata, et al., Palbociclib in hormone-receptor–Positive advanced breast cancer, N. Engl. J. Med. 373 (2015) 209–219, https://doi.org/10.1056/NEJMoa1505270.

[12] M. Cristofanilli, N.C. Turner, I. Bondarenko, J. Ro, S.-A. Im, N. Masuda, et al., Fulvestrant plus palbociclib versus fulvestrant plus placebo for treatment of hormone-receptor-positive, HER2-negative metastatic breast cancer that progressed on previous endocrine therapy (PALOMA-3): final analysis of the multicentre, double-blind, phase 3 randomised controlled trial, Lancet Oncol. 17 (2016) 425–439, https://doi.org/10.1016/S1470-2045(15)00613-0.

[13] D.J. Wood, J.A. Endicott, Structural insights into the functional diversity of the CDK–cyclin family, Open. Biol. 8 (2018) 180112, https://doi.org/10.1098/rsob.180112.

[14] M. Malumbres, Cyclin-dependent kinases, Genome Biol. 15 (2014) 122, https://doi.org/10.1186/gb4184.

[15] S. Dalton, P.D. Coverdell, Linking the cell cycle to cell fate decisions, Trends. Cell Biol. 25 (2015) 592–600, https://doi.org/10.1016/j.tcb.2015.07.007.

[16] P.J. Roberts, J.E. Bisi, J.C. Strum, A.J. Combest, D.B. Darr, J.E. Usary, et al., Multiple roles of cyclin-dependent kinase 4/6 inhibitors in cancer therapy, J. Natl. Cancer Inst. 104 (2012) 476–487, https://doi.org/10.1093/jnci/djs002.

[17] E. Hamilton, J.R. Infante, Targeting CDK4/6 in patients with cancer, Cancer Treat. Rev. 45 (2016) 129–138, https://doi.org/10.1016/j.ctrv.2016.03.002.

[18] S. Qian, Q.L. Chen, J.L. Guan, Y. Wu, Z.Y. Wang, Synthesis and biological evaluation of Raddeanin A, a triterpene saponin isolated from Anemone raddeana, Chem. Pharm. Bull. 62 (2014) 779–785, https://doi.org/10.1248/cpb.c14-00138.

[19] Q. Wang, J. Mo, C. Zhao, K. Huang, M. Feng, W. He, J. Wang, S. Chen, Z. Xie, J. Ma, S. Fan, Raddeanin A suppresses breast cancer-associated osteolysis through inhibiting osteoclasts and breast cancer cells, Cell Death. Dis. 9 (3) (2018) 376, https://doi.org/10.1038/s41419-018-0417-0.

[20] J.-N. Li, Y. Yu, Y.-F. Zhang, Z.-M. Li, G.-Z. Cai, J.-Y. Gong, Synergy of Raddeanin A and cisplatin induced therapeutic effect enhancement in human hepatocellular carcinoma, Biochem. Biophys. Res. Commun. 485 (2017) 335–341, https://doi.org/10.1016/j.bbrc.2017.02.079.

[21] Y. Teng, J. Li, S. Liu, X. Zou, L. Fang, J. Zhou, et al., Autophagy protects from Raddeanin A-induced apoptosis in SGC-7901 Human gastric cancer cells, Evid. Based. Complement. Alternat. Med. 2016 (2016) 9406758, https://doi.org/10.1155/2016/9406758.

[22] C. Meng, Y. Teng, X. Jiang, Raddeanin A induces apoptosis and cycle arrest in Human HCT116 cells through PI3K/AKT pathway regulation In Vitro and In vivo, Evid. Based. Complement. Alternat. Med. 2019 (2019) 7457105, https://doi.org/10.1155/2019/7457105.

[23] X. Shen, L. Li, Y. He, X. Lv, J. Ma, Raddeanin A inhibits proliferation, invasion, migration and promotes apoptosis of cervical cancer cells via regulating miR-224-3p/Slit2/Robo1 signaling pathway, Aging (Albany. NY) 13 (2021) 7166–7179, https://doi.org/10.18632/aging.202574.

[24] L. Li, M. Chen, G. Li, R. Cai, Raddeanin A induced apoptosis of non-small cell lung cancer cells by promoting ROS-mediated STAT3 inactivation, Tissue and Cell 71 (2021) 101577, https://doi.org/10.1016/j.tice.2021.101577.

[25] Y. Xing, W. Xue, Y. Teng, Z. Jin, X. Tang, Z. Li, et al., Raddeanin A promotes autophagy-induced apoptosis by inactivating PI3K/AKT/mTOR pathway in lung adenocarcinoma cells, Naunyn-Schmiedeberg's Arch. Pharmacol. 396 (2023) 1987–1997, https://doi.org/10.1007/s00210-023-02447-z.

[26] A. Daina, O. Michielin, V. Zoete, SwissTargetPrediction: updated data and new features for efficient prediction of protein targets of small molecules, Nucleic. Acids. Res. 47 (2019) W357–W364, https://doi.org/10.1093/nar/gkz382.

[27] D. Gfeller, O. Michielin, V. Zoete, Shaping the interaction landscape of bioactive molecules, Bioinformatics. 29 (23) (2013) 3073–3079, https://doi.org/10.1093/bioinformatics/btt500.

[28] S. Nebenfuehr, K. Kollmann, V. Sexl, The role of CDK6 in cancer, Int. J. Cancer 147 (2020) 2988–2995, https://doi.org/10.1002/ijc.33054.

[29] M. Wang, R.S. Herbst, C. Boshoff, Toward personalized treatment approaches for non-small-cell lung cancer, Nat. Med. 27 (2021) 1345–1356.

[30] C.M. Blakely, T.B.K. Watkins, W. Wu, B. Gini, J.J. Chabon, C.E. McCoach, et al., Evolution and clinical impact of co-occurring genetic alterations in advanced-stage EGFR-mutant lung cancers, Nat. Genet. 49 (2017) 1693–1704, https://doi.org/10.1038/ng.3990.

[31] Q.-Y. Chong, Z.-H. Kok, N.-L.-C. Bui, X. Xiang, A.L.-A. Wong, W.-P. Yong, et al., A unique CDK4/6 inhibitor: current and future therapeutic strategies of abemaciclib, Pharmacol. Res. 156 (2020) 104686, https://doi.org/10.1016/j.phrs.2020.104686.

[32] W. Gong, L. Wang, Z. Zheng, W. Chen, P. Du, H. Zhao, Cyclin-dependent kinase 6 (CDK6) is a candidate diagnostic biomarker for early non-small cell lung cancer, Transl. Cancer Res. 9 (2020) 95–103, https://doi.org/10.21037/tcr.2019.11.21.

[33] A. Patnaik, L.S. Rosen, S.M. Tolaney, A.W. Tolcher, J.W. Goldman, L. Gandhi, K. P. Papadopoulos, M. Beeram, D.W. Rasco, J.F. Hilton, A. Nasir, R.P. Beckmann, A. E. Schade, A.D. Fulford, T.S. Nguyen, R. Martinez, P. Kulanthaivel, L.Q. Li, M. Frenzel, D.M. Cronier, E.M. Chan, K.T. Flaherty, P.Y. Wen, G.I. Shapiro, Efficacy and safety of Abemaciclib, an inhibitor of CDK4 and CDK6, for patients with breast cancer, non-small cell lung cancer, and other solid tumors, Cancer Discov. 6 (7) (2016) 740–753, https://doi.org/10.1158/2159-8290.CD-16-0095.

[34] S.R.D. Johnston, M. Toi, J. O'Shaughnessy, P. Rastogi, M. Campone, P. Neven, et al., Abemaciclib plus endocrine therapy for hormone receptor-positive, HER2-negative, node-positive, high-risk early breast cancer (monarchE): results from a preplanned interim analysis of a randomised, open-label, phase 3 trial, Lancet Oncol. 24 (2023) 77–90, https://doi.org/10.1016/S1470-2045(22)00694-5.

[35] S. Goel, J.S. Bergholz, J.J. Zhao, Targeting cyclin-dependent kinases 4 and 6 in cancer, Nat. Rev. Cancer 22 (2022) 356–372, https://doi.org/10.1038/s41568-022-00456-3.

[36] G. Gu, H. Qi, T. Jiang, B. Ma, Z. Fang, H. Xu, et al., Investigation of the cytotoxicity, apoptosis and pharmacokinetics of Raddeanin A, Oncol. Lett. 13 (2017) 1365–1369, https://doi.org/10.3892/ol.2017.5588.